Bing Jiang
Yongqiao Wei ✉
Shaojiang Wang
Jianquan Zhang
Dengqiu Ma
Lan Luo
Jianbing Long

https://doi.org/10.21278/TOF.501070024
ISSN 1333-1124
eISSN 1849-1391

THE MESHING STIFFNESS CHARACTERISTICS OF VARIABLE HYPERBOLIC CIRCULAR ARC TOOTH TRACE CYLINDRICAL GEARS UNDER INSTALLATION ERRORS

Summary

To investigate the impact of installation errors on the meshing performance of variable hyperbolic circular arc tooth trace (VH-CATT) cylindrical gear transmission systems, this study examines the time-varying meshing stiffness characteristics under the influence of such errors. First, based on the VH-CATT cylindrical gear forming principle, a precise three-dimensional model was established after deriving tooth surface equations. Second, the tooth face load and meshing stiffness of VH-CATT cylindrical gears were calculated using tooth contact analysis (TCA) and load tooth contact analysis (LTCA) models. Finally, the effects of different mounting errors on the meshing stiffness of VH-CATT cylindrical gears were examined. The study conclusively shows that the centre distance installation error, the axial installation error, and the rotational installation error around the gears' centre line direction (for the y-axis) exert a pronounced effect on both the single-tooth stiffness and the meshing stiffness characteristics of VH-CATT cylindrical gears. The rotational installation error around the normal direction of the gear centre line (for the x-axis) notably affects the single-tooth stiffness characteristics of the VH-CATT cylindrical gears, yet it exhibits limited sensitivity towards the meshing stiffness characteristics. These findings provide a technical basis for reducing vibration and noise, improving load carrying capacity, and optimising the tooth surface design of VH-CATT cylindrical gears.

Key words: *variable hyperbolic circular arc tooth trace cylindrical gear; load tooth contact analysis; installation error; meshing stiffness.*

1. Introduction

The VH-CATT cylindrical gear is a newly proposed cylindrical gear. The middle cross-section boasts a tooth profile curve that conforms to a theoretical involute, while the parallel end-face tooth profile curves, aligned with the middle cross-section, are enveloped by diverse hyperbolas. The direction of the tooth line follows an arc-shaped curve [1]. Zhao devised a

comprehensive approach to determining the parameter range spanning the entire tooth surface, thereby facilitating the formulation of an all-inclusive tooth surface equation for VH-CATT cylindrical gears [2]. Zhang developed a range of modular division schemes to facilitate the rapid design of the machine tool in accordance with the functional requirements of the rotary cutter head cutting machine tool [3-4]. Wu investigated the influence of machine tool errors on machined tooth surfaces, deriving the error tooth surface equation. In addition, he pioneered the establishment of an LTCA model tailored specifically for VH-CATT cylindrical gears [5-7]. Guo proposed an analytical solution method aimed at investigating the influence of various parameters on the contact ellipse of VH-CATT cylindrical gears [8]. Liu conducted a tooth contact analysis specifically targeted at the modified VH-CATT cylindrical gears. The author's analysis aimed at evaluating the contact behaviour and performance of gears after undergoing the modification process [9]. Liang analysed the kinematic relationship between the spindle and cutter head of the machine tool based on cutting principles and investigated the motion stability of the spindle-cutter head system. Additionally, the study explored the impact of geometric error sources on the errors in the tooth surface of the gears processed by the specialised VH-CATT gear machine [10-11]. Wei proposed a comprehensive tooth surface wear prediction model specifically tailored for VH-CATT cylindrical gears, and studied the variation patterns of tooth surface wear that take into account assembly errors. This work significantly advances the understanding and prediction of the durability and performance of such gears under real-world operating conditions [12-13]. Ma analysed the meshing impact characteristics of VH-CATT gear, performed design modifications to the tooth surface, and conducted a contact analysis for the modified gear [14-17]. In summary, significant progress has been made in VH-CATT cylindrical gears, particularly in tooth surface forming methods, contact properties, manufacturing and tooth surface wear, and notably in meshing properties and forming methods.

Installation errors in gears can adversely affect their meshing capability, subsequently leading to increased vibration and noise within the system. Consequently, investigating the impact of installation errors on the meshing performance of gears is instrumental in mitigating noise and vibration in gear systems. Luo introduced a novel kinematic model for gear meshing, and, based on this model, he calculated the meshing stiffness of both healthy and faulty gears under the assumptions of standard installation and time-varying errors in the centre distance between gears [18]. Ahmed Shehata utilised three different pieces of software to analyse variation in the contact position and root stress of helical gears caused by misalignment and tooth profile deviation [19]. Paras Kumar conducted experimental research to examine how installation mistakes affect the gear contact area and failure mechanisms [20-21]. Lü carried out a tooth surface load contact analysis on drum gears with installation errors [22]. Song conducted a study on the impact of machine tool installation errors on the meshing performance of small module spiral bevel gears [23]. Zhao analysed the meshing characteristics of modified spur gear pairs under various assembly error conditions. The study delved into the intricate relationships between assembly errors, the tooth modification parameters, and their combined effects on the meshing behaviour of the gear pairs [24]. The study of VH-CATT cylindrical gears under installation errors has a solid theoretical and technological foundation thanks to the aforementioned studies on the meshing performance of gear transmission systems taking installation errors into consideration.

Meshing stiffness plays a crucial role as an excitation parameter in the strength assessment and dynamic analysis of gear structures [25-27], serving as the primary source of vibration and noise, thus exerting significant influence on the performance of gear transmission systems. Currently, the calculation methods for gear meshing stiffness primarily include the experimental method, the finite element method, and the analytical method. This

experimental methodology requires sophisticated equipment, specialised measurement techniques, and stringent hardware demands. When employing a finer mesh of a larger scale along with appropriate boundary conditions, the finite element method (FEM) yields results that are more accurate and reliable, frequently serving as a benchmark for comparison and validation against other methodologies. However, it is characterised by lengthy calculation processes and limited generalisability of the model. While analytical methods offer high precision, there are significant challenges in further enhancing the accuracy of gear stiffness, particularly when calculating the meshing stiffness of gears with complex tooth surface structures. The complexity of such calculations is a formidable challenge. Marafona João proposed a model for the fast and accurate calculation of meshing stiffness under asymmetric tooth pairs, using extensive simulations to evaluate how asymmetry affects the meshing stiffness, dynamic displacement, and load distribution of the gears [28]. Pedrero José developed a computational model to determine gear mesh stiffness through the precise calculation of contact line length. This effectively led to improvements in the precision of mesh stiffness calculations [29]. Wen devised an innovative analytical algorithm grounded in the slicing method, enabling the precise calculation of meshing stiffness in gears of variable thickness. To validate the veracity of this approach, the author used the finite element method, which subsequently underwent rigorous error analysis to ensure its accuracy [30]. Zou established an iterative model for meshing stiffness that takes into account variation in the mesh phase difference caused by angular misalignment errors [31]. Liu proposed a meshing stiffness and transmission error correction algorithm for helical gears, taking into consideration the root transition curve [32]. Cai employed a hybrid approach that integrates differential equations with finite element methods to solve mesh stiffness under various conditions of tooth surface roughness [33]. To accurately calculate the mesh stiffness of spiral bevel gears under various operating conditions, scholars have independently proposed diverse methodologies. Each of these approaches aims to address the complexity and specificity of the gear system, ensuring that the resulting mesh stiffness calculations are precise [34-35]. Sánchez Miryam performed detailed calculations to quantify the mesh stiffness of profile-modified spur gears, taking into account the influence of surface wear [36]. The researchers mentioned have devised diverse methodologies for assessing gear mesh stiffness, predominantly centring on conventional gears such as spur, helical, and spiral bevel types. Nevertheless, there is a notable gap in the literature concerning the mesh stiffness analysis of gears featuring intricate tooth surface geometries. The aforementioned investigative approaches serve as a valuable theoretical and technical framework for computing the mesh stiffness of VH-CATT cylindrical gears, taking into account potential installation errors.

While numerous researchers have extensively studied the meshing performance of gears considering installation errors, relatively few studies have focused specifically on the influence of these errors on mesh stiffness characteristics. This is particularly evident in the case of complex tooth surface structures like those found in VH-CATT cylindrical gears, where investigations into how installation errors affect their mesh stiffness properties remain limited. To address this gap, this paper proposes a method for calculating the meshing stiffness of VH-CATT cylindrical gears by integrating the TCA model with the LTCA model. Furthermore, the study concludes with an analysis of the impact of axial installation errors, centre distance installation errors, rotational installation errors around the gear centre line direction (for the y-axis), and rotational installation errors around the normal direction of the gear centre line (for the x-axis) on the meshing stiffness of VH-CATT cylindrical gears.

2. Accurate modelling of VH-CATT cylindrical gears

The coordinate system of the VH-CATT cylindrical gear machine tool system is illustrated in Fig. 1, where $O_1 - x_1y_1z_1$ is the tool static coordinate system; $O_c - x_cy_cz_c$ is the coordinate system of the big cutting tool disc movement; $O_i - x_iy_iz_i$ signifies the static coordinate system of the gear blank, while $O_d - x_dy_dz_d$ represents the dynamic coordinate system of the same gear blank; R_i is the radius of the indexing circle of the processed gear; R_T is the tooth line radius; φ_i is the rotational angle of the gear to be machined in the machining process; θ_i is the rotation angle of the cutterhead; and ω_1 and ω_2 represent the rotational angular velocities of the cutting tool and the gear blank, respectively.

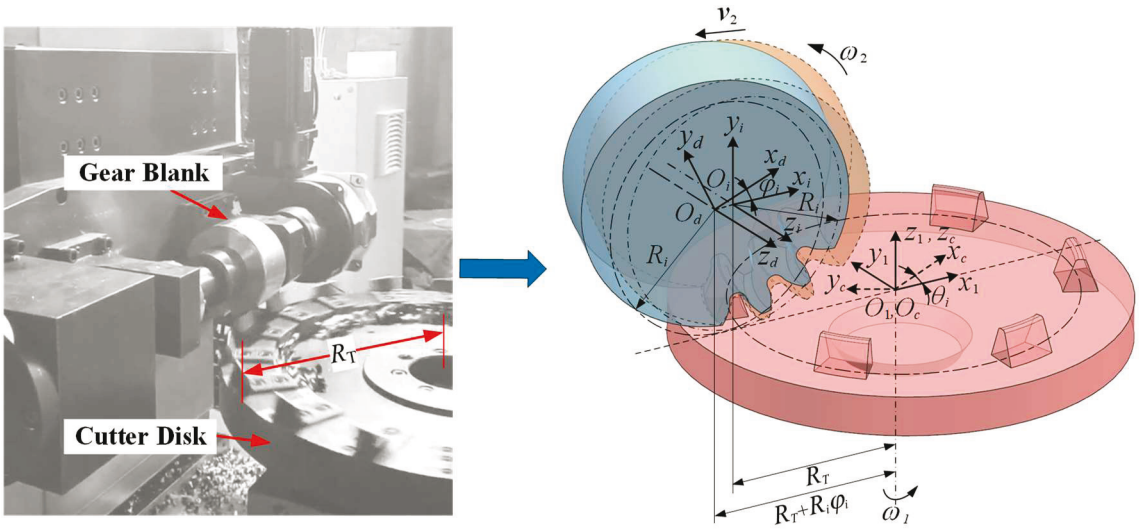

Fig. 1 VH-CATT cylindrical gear machining coordinate system

Using the principles of gear meshing and the relative motion between the cutting tool and the gear blank, the position vector of the cutting tool is transformed from the coordinate system $O_1 - x_1y_1z_1$ to the coordinate system $O_d - x_dy_dz_d$, which is fixed to the gear being processed. Based on the detailed derivation process outlined in reference [2], Eq. (1) expresses the tooth surface equation of the VH-CATT cylindrical gear in the coordinate system $O_d - x_dy_dz_d$:

$$\begin{cases} x_d = \left[-A\cos\theta_i + R_T + R_i\varphi_i\right]\cos\varphi_i + \left(u_i\cos\alpha - R_i\right)\sin\varphi_i \\ y_d = \left[A\cos\theta_i - R_T - R_i\varphi_i\right]\sin\varphi_i + \left(u_i\cos\alpha - R_i\right)\cos\varphi_i \\ z_d = A\sin\theta_i \\ A = \mp u_i\sin\alpha + R_T \pm \dfrac{\pi}{4}m \\ u_i = \pm\sin\alpha\dfrac{\cos\theta_i\left(R_T \pm \dfrac{\pi}{4}m\right) - \left(R_i\varphi_i + R_T\right)}{\cos\theta_i} \end{cases} \tag{1}$$

where α is the pressure angle; m is modulus; u_i is the distance between a point on the cutter surface and the pitch point along the generatrix direction.

According to Eq. (1), the selected gear design parameters are as follows: tooth number z_1=29, z_2=41, modulus m=8 mm, pressure angle α=20°, tooth width B=80 mm, cutter radial R_T=200 mm. MATLAB is used to create the mathematical model of the gear tooth's tooth

flank, as shown in Fig. 2. The MATLAB calculation data were imported into UG three-dimensional modelling software for three-dimensional solid modelling and for the obtained 3D, as shown in Fig. 3.

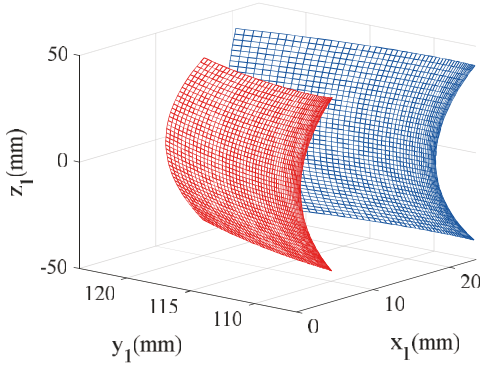

Fig. 2 Point cloud of tooth surface

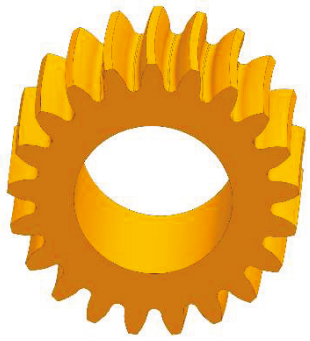

Fig. 3 Three-dimensional model

3. Tooth contact analysis model of the VH-CATT cylindrical gear

In the process of analysing the meshing contact between gear tooth surfaces, it is essential to transform the equations of the tooth surfaces into a unified coordinate system through coordinate transformations so as to ensure accurate meshing between the pinion and the gear. To establish a TCA model for the VH-CATT cylindrical gear that accounts for mounting errors, a coordinate system for gear pair meshing that takes into account such errors is established as in Fig. 4, where $O_p - x_p y_p z_p$ is the fixed coordinate system of the pinion without installation error; $O_e - x_e y_e z_e$ represents the pinion's coordinate system after incorporating the centre distance installation error De; $O_a - x_a y_a z_a$ represents the pinion's coordinate system after incorporating the axial installation error Da; $O_n - x_n y_n z_n$ is the pinion dynamic coordinate system; $O_g - x_g y_g z_g$ is the gear fixed coordinate system without installation error; $O_y - x_y y_y z_y$ is the coordinate system after the installation error β_y of the gear rotational around the y-axis; $O_x - x_x y_x z_x$ is the coordinate system after the installation error β_x of the gear rotational around the x-axis; $O_m - x_m y_m z_m$ is the gear dynamic coordinate system. M denotes the instantaneous meshing point between the gear pair, while $\boldsymbol{n}$ represents the common normal vector to this instantaneous meshing point. ψ_p and ψ_g represent the engagement angles of the pinion and the gear, respectively; R_p and R_g respectively represent the pitch radius of the pinion and the gear.

In the relative position relationship between coordinate systems as in Fig. 4, the corresponding coordinate transformation matrix is introduced to obtain the conditions for achieving continuous cutting and touching of the two tooth surfaces, as shown in Eqs. (2) and (3):

$$\begin{cases} \boldsymbol{r}_{np}\left(\psi_p,\theta_n,\varphi_n\right) = \boldsymbol{M}_{pn}\left(\psi_p\right)\cdot\boldsymbol{r}_n\left(\theta_n,\varphi_n\right) \\ \boldsymbol{n}_{np}\left(\psi_p,\theta_n,\varphi_n\right) = \boldsymbol{L}_{pn}\left(\psi_p\right)\cdot\boldsymbol{n}_n\left(\theta_n,\varphi_n\right) \end{cases} \tag{2}$$

$$\begin{cases} \boldsymbol{r}_{mp}\left(\psi_g,\theta_m,\varphi_m\right) = \boldsymbol{M}_{pm}\left(\psi_g\right)\cdot\boldsymbol{r}_m\left(\theta_m,\varphi_m\right) \\ \boldsymbol{n}_{mp}\left(\psi_g,\theta_m,\varphi_m\right) = \boldsymbol{L}_{pm}\left(\psi_g\right)\cdot\boldsymbol{n}_m\left(\theta_m,\varphi_m\right) \end{cases} \tag{3}$$

where $\boldsymbol{M}_{pn}$ and $\boldsymbol{L}_{pn}$ are the transformation matrices from the coordinate system $O_n - x_n y_n z_n$ to the coordinate system $O_p - x_p y_p z_p$, as shown in Eqs. (4) and (5); $\boldsymbol{M}_{pm}$ and $\boldsymbol{L}_{pm}$ are the transformation matrices from the coordinate system $O_m - x_m y_m z_m$ to the coordinate system $O_p - x_p y_p z_p$, as shown in Eqs. (6) and (7).

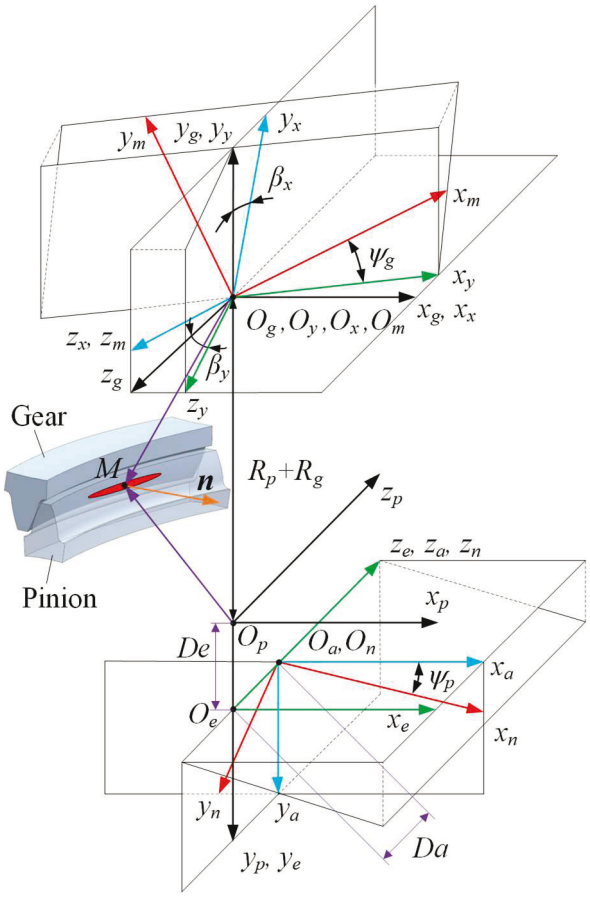

Fig. 4 Meshing coordinate system of gear pair under installation errors.

$$\boldsymbol{M}_{pn} = \begin{bmatrix} \cos\psi_p & \sin\psi_p & 0 & 0 \\ -\sin\psi_p & \cos\psi_p & 0 & De \\ 0 & 0 & 1 & Da \\ 0 & 0 & 0 & 1 \end{bmatrix} \tag{4}$$

$$\boldsymbol{L}_{pn} = \begin{bmatrix} \cos\psi_p & \sin\psi_p & 0 \\ -\sin\psi_p & \cos\psi_p & 0 \\ 0 & 0 & 1 \end{bmatrix} \tag{5}$$

$$\boldsymbol{M}_{pm} = \begin{bmatrix} \cos\beta_y\cos\psi_g & -\cos\beta_y\sin\psi_g & -\sin\beta_y & 0 \\ \cos\beta_x\sin\psi_g & \cos\beta_x\cos\psi_g & -\sin\beta_x\cos\beta_y & R_1+R_2 \\ -\sin\beta_x\sin\beta_y\cos\psi_g & +\sin\beta_x\sin\beta_y\sin\psi_g & & \\ \sin\beta_x\sin\psi_g & \sin\beta_x\cos\psi_g - & \cos\beta_x\cos\beta_y & 0 \\ +\cos\beta_x\sin\beta_y\cos\psi_g & \cos\beta_x\sin\beta_y\sin\psi_g & & \\ 0 & 0 & 0 & 1 \end{bmatrix} \tag{6}$$

$$\boldsymbol{L}_{pm}=\begin{bmatrix} \cos\beta_y\cos\psi_g & -\cos\beta_y\sin\psi_g & -\sin\beta_y \\ \cos\beta_x\sin\psi_g & \cos\beta_x\cos\psi_g & \\ -\sin\beta_x\sin\beta_y\cos\psi_g & +\sin\beta_x\sin\beta_y\sin\psi_g & -\sin\beta_x\cos\beta_y \\ \sin\beta_x\sin\psi_g & \sin\beta_x\cos\psi_g & \\ +\cos\beta_x\sin\beta_y\cos\psi_g & -\cos\beta_x\sin\beta_y\sin\psi_g & \cos\beta_x\cos\beta_y \end{bmatrix} \tag{7}$$

Therefore, the mathematical model of tooth contact analysis expressed in the coordinate system $O_p-x_py_pz_p$ can be obtained as shown in Eq. (8):

$$\begin{cases} \boldsymbol{r}_{np}\left(\psi_p,\theta_n,\varphi_n\right)=\boldsymbol{r}_{mp}\left(\psi_g,\theta_m,\varphi_m\right) \\ \boldsymbol{n}_{np}\left(\psi_p,\theta_n,\varphi_n\right)=\boldsymbol{n}_{mp}\left(\psi_g,\theta_m,\varphi_m\right) \end{cases}. \tag{8}$$

By inputting the engagement angle of the pinion ψ_p, Eq. (8) and the specific results of θ_n, φ_n, θ_m, φ_m, and ψ_g can be solved. Then, the coordinates of the contact points on the two meshing tooth surfaces and the normal vectors at the contact points can be determined.

4. Load tooth contact analysis mathematical model

Load Tooth Contact Analysis (LTCA) is an important gear design technology. Before the trial production of gear products, high-precision computer simulation of the meshing process of gears under load is carried out to obtain the working performance of the designed gears under quasi-real working conditions.

The tooth contact deformation model is shown in Fig. 5. Fig. 5(a) shows the single-tooth pair contact deformation, and Fig. 5(b) is the double-tooth pair contact deformation. Σ_1 is the pinion tooth surface, Σ_2 is the gear tooth surface, and M is the meshing point. After the gear teeth are loaded, the contact line can be regarded as the contact of numerous points. j and j' represent arbitrary discrete points on the instantaneous contact line between the two tooth surfaces, and w_j represents the normal clearance at that specific point. F_j and $F_{j'}$ denote the normal loads, and the contact deformation under the influence of load P is represented by u_j and $u_{j'}$. When a gear is subjected to a load P, it undergoes a normal displacement denoted by s_z. According to reference [37], the deformation compatibility equation pertaining to the scatter point j can be elegantly formulated as:

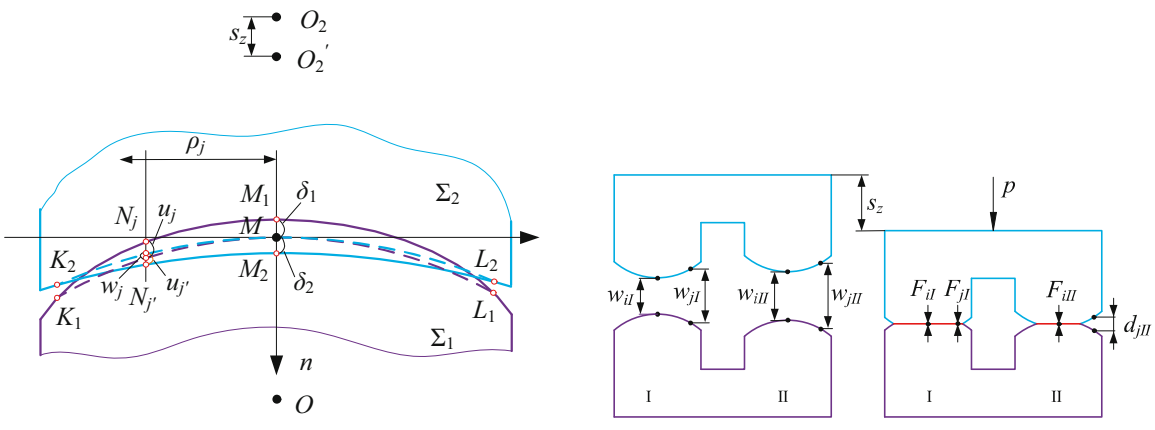

(*a*) Contact deformation of a single-tooth pair (*b*) Contact deformation of a double-tooth pair

Fig. 5 Gear load contact deformation model

$$\left(\sum_{k=1}^{n} f_{jk} + \sum_{k=1}^{n} f_{j'k'}\right) F_k + w_j = s_z + d_j, \tag{9}$$

where d_j represents the residual clearance of the tooth surface. In the scenario where the tooth surface comes into contact at the discrete point j, it follows that $d_j = 0$, $F_j > 0$. Conversely, if there is no contact at the discrete point j, then $d_j > 0$, $F_j = 0$. The compliance coefficients of the main driven gear are denoted by f_{jk} and $f_{j'k'}$, respectively.

Considering multiple-tooth contact, the comprehensive deformation compatibility equation is elegantly formulated in a matrix representation as:

$$\boldsymbol{S}_h \boldsymbol{F}_h + \boldsymbol{w}_h = s_z \boldsymbol{e} + \boldsymbol{d}_h, h = \mathrm{I}, \mathrm{II}\ , \tag{10}$$

where $\boldsymbol{S}$ denotes the flexibility matrix of the tooth surface contact points, $\boldsymbol{F}$ represents the load matrix applied to the contact points, $\boldsymbol{w}$ is the initial clearance matrix of the tooth surface prior to deformation, $\boldsymbol{d}$ signifies the residual gap matrix after deformation at the tooth surface's contact points, and h stands for the total number of teeth in contact.

The tooth surface flexibility matrix is one of the key technologies of gear load contact analysis. This study utilises a secondary development approach that combines ABAQUS and MATLAB to establish a finite element model. Through this model, the flexibility coefficients of the tooth surface after loading are calculated, enabling the derivation of the flexibility matrix for the nodes on the tooth surface. Subsequently, a hybrid interpolation method based on the principle of virtual work is adopted to calculate the flexibility matrix of the discrete contact points on the major axis of the instantaneous contact ellipse. The specific and detailed interpolation process is described in references [7,37].

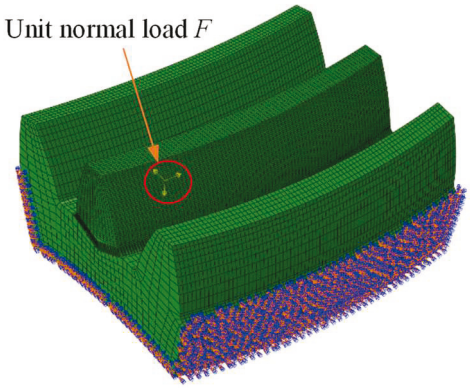

Fig. 6 Node load

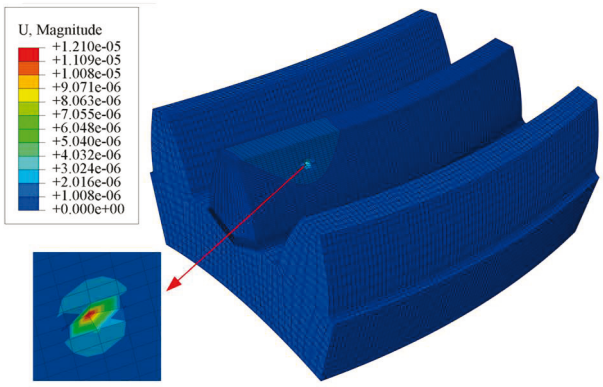

Fig. 7 Tooth surface node deformation

Fig. 6 shows the unit normal load applied on the tooth surface node of the gear, and Fig. 7 is the tooth surface node deformation. The primary modelling procedures and parameter configurations for the finite element model are as follows:

1. Material properties: The master and slave gears have a density of 7.8×10^{-9} T/mm³, Young's modulus of 2.1×10^{5} MPa, and Poisson's ratio of 0.3.
2. Element type definition: Hexahedral linear reduced-integration elements (C3D8R) are utilised.
3. Analysis settings: An implicit static analysis algorithm is employed with large deformation enabled. The initial time step size is set to 0.001.
4. Meshing: For the tooth profile direction, the mesh size in areas of tooth surface contact and tooth root regions is specified as 0.06 mm, while the mesh size in the tooth width direction is set to 2 mm.

5. Boundary conditions: Coupling constraints are established between the gear's rotational centre and its inner cylinder. The boundary conditions are applied at the coupling point to constrain all degrees of freedom of the gear.
6. Load application: A unit load of 1 N normal force is applied to the nodes on the meshed tooth surface of the second gear tooth, as illustrated in the established finite element model.

Based on the principles of non-embedding, force equilibrium, and deformation compatibility, a mathematical model was constructed to represent the contact equilibrium state of tooth surfaces under loading conditions:

$$\begin{cases} f = \min\left[\dfrac{1}{2}\left(\boldsymbol{P}^T \boldsymbol{S}\right)\boldsymbol{P}\right] \\ \boldsymbol{w}_h = -\boldsymbol{S}_h \boldsymbol{F}_h + s_z \boldsymbol{e} + \boldsymbol{d}_h, h = \mathrm{I}, \mathrm{II} \\ T = \sum_{i=0}^{n}\left(\boldsymbol{d}_{i\mathrm{I}} \boldsymbol{n}_{\mathrm{I}} \boldsymbol{F}_{i\mathrm{I}} + \boldsymbol{d}_{i\mathrm{II}} \boldsymbol{n}_{\mathrm{II}} \boldsymbol{F}_{i\mathrm{II}}\right) \\ S.t: d_j > 0 (d_j = 0) \left\| F_j = 0\left(F_j > 0\right), s_z \geq 0, F_j \geq 0 \right. \end{cases} \tag{11}$$

where $\boldsymbol{P}$= [$\boldsymbol{F}_{\mathrm{I}}$; $\boldsymbol{F}_{\mathrm{II}}$]; $\boldsymbol{S}$= [$\boldsymbol{S}_{\mathrm{I}}$ 0; 0 $\boldsymbol{S}_{\mathrm{II}}$]; j= 1, 2,..., 2n.

The reduction of the transmission system's deformation energy is the goal of nonlinear programming. The parameters $\boldsymbol{S}$, $\boldsymbol{w}$, T and $\boldsymbol{n}$ in Eq. (11) are known parameters, and the parameters to be solved are $\boldsymbol{P}$, s_z and $\boldsymbol{d}$. Based on the discrete load calculated by the nonlinear mathematical programming model, Eq. (12) can be used to compute the contact tooth pair's instantaneous load distribution coefficient L_h:

$$L_h = \frac{\sum_{j=1}^{n} F_{jh}}{p} \quad h=\mathrm{I},\mathrm{II}\ . \tag{12}$$

After applying a load of T = 1000 N·m to the gear pair, the computational results reveal the load distribution across the tooth surface as depicted in Fig. 8, with the maximum load highlighted in Fig. 9. Based on the analysis of the load distribution on the tooth surface, it can be observed that the load in the single-tooth mesh area (I) is significantly higher than that in the double-tooth mesh area (II-1 and II-2), with the load being concentrated towards the middle of the tooth width.

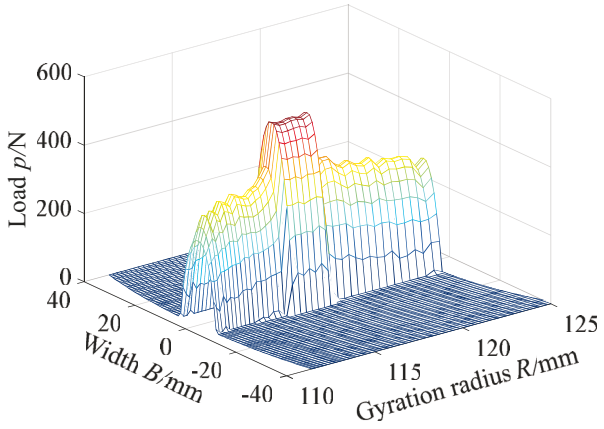

Fig. 8 Load distribution on tooth surface

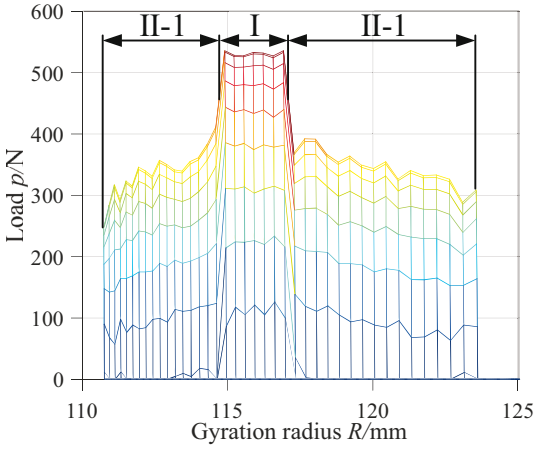

Fig. 9 Tooth surface maximum load

5. Meshing stiffness calculation of the VH-CATT cylindrical gear

The time-varying meshing stiffness represents the combined stiffness of all pairs of teeth engaged in a complete meshing cycle. Due to the continuous nature of gear transmission, the number of meshing teeth constantly varies between one and two over time, leading to corresponding changes in the meshing stiffness during each meshing period. The definition of mesh stiffness refers to the proportionality coefficient, which describes the direct proportionality between the normal load applied to the gear teeth and the normal deformation displacement of the gear teeth within the elastic range. Therefore, the mesh stiffness k can be derived from the ratio of the normal load p along the contact line to the normal contact deformation s_z within one engagement cycle, as shown in Eq. (13). The values of p and s_z in the equation can be computed using LTCA. The calculation process is shown in Fig. 10.

$$k = \frac{p}{s_z} \tag{13}$$

The LTCA analysis results indicate that the normal deformation of multiple pairs of tooth meshing simultaneously is consistent due to the deformation coordination conditions. Additionally, the tooth surface loads involved in the meshing gear are different due to the varying flexibility coefficients of different contact points. Utilising both Eq. (13) and Eq. (12), it is possible to calculate the single-tooth stiffness k_s during the meshing and disengagement process of the gear teeth.

$$k_s = L_h \frac{p}{s_z} \tag{14}$$

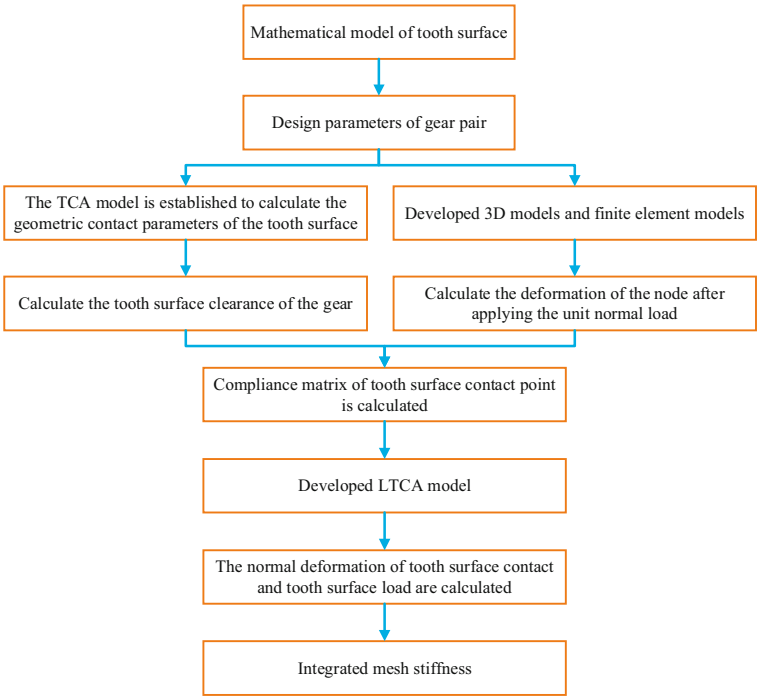

Fig. 10 Comprehensive stiffness calculation process

Fig. 11 represents the comprehensive meshing stiffness of the VH-CATT cylindrical gear in a complete meshing period calculated accurately by the LTCA methodology. This stiffness displays a discernible periodic variation pattern, with notably higher values observed in the double-tooth meshing area compared to the single-tooth meshing area. The transition between these two areas is marked by a distinct and sudden change in the stiffness profile. Fig. 12 shows

the single-tooth stiffness behaviour. Notably, the stiffness increases progressively as the rotational angle rises in the tooth root region, whereas it experiences a gradual decline with an increase in the rotational angle towards the tooth tip area. The single-tooth stiffness is the maximum in the middle region, and the fluctuation range is not large. The results are consistent with the theoretical analysis.

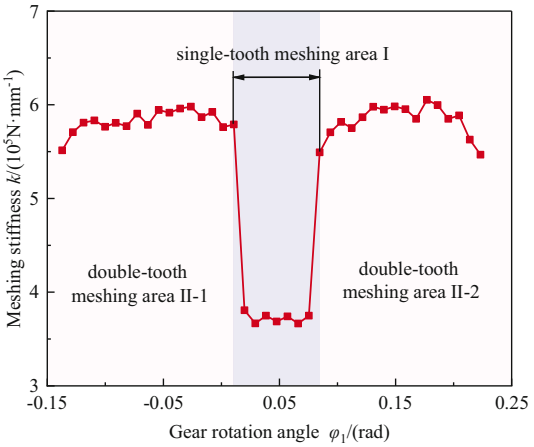

Fig. 11 Meshing stiffness

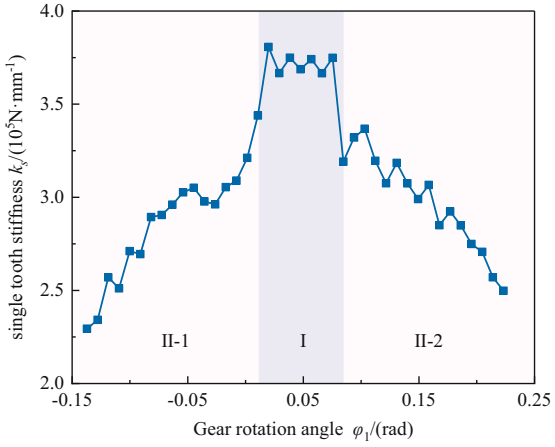

Fig. 12 Single-tooth stiffness

6. The influences of installation error on VH-CATT cylindrical gear stiffness

6.1 The influence of the centre distance installation error *De* on meshing stiffness

Fig. 13 is the load distribution when *De* = 3 mm. Figs. 14 and 15 are the impact of *De* (with values of 1 mm, 2 mm, and 3 mm, respectively) on both the single-tooth stiffness and the meshing stiffness of the VH-CATT cylindrical gear. As shown in the figure, when the gear pair is assembled taking into account the centre distance installation error, there will be a lag phenomenon when the gear teeth begin to enter the meshing, that is, the actual meshing line decreases. The hysteresis phenomenon entering the meshing becomes increasingly evident as *De* increases, and the real meshing line shrinks as *De* increases. Furthermore, the gear tooth's single-tooth meshing area grows as *De* does.

Based on Figs. 14 and 15, it is evident that as *De* increases, both the single-tooth stiffness and the meshing stiffness exhibit a decreasing trend. Fig. 16 depicts the average reduction amplitude of meshing stiffness. In the area II-1, the average reduction amplitudes are 4.81%, 8.14%, and 11.75%, respectively. In area I, the average reduction amplitudes are 2.99%, 6.38%, and 10.17%, respectively. Additionally, in area II-2, the average reduction amplitudes are 5.14%, 7.59%, and 12.32%, respectively.

The aforementioned phenomenon can be traced back to the increased centre distance during the installation process of the pinion and gear, which in turn results in an enlargement of the backlash between the two components. The pinion must rotate by a certain angle to come into contact with the gear. As the backlash increases, the second pair of gear teeth undergoes delayed meshing, leading to a reduction in the simultaneous meshing time of the two tooth pairs. Consequently, the double-tooth meshing area diminishes, while the single-tooth meshing area grows. Furthermore, an increase in the centre distance installation error results in greater gear tooth side clearance and heightened tooth contact deformation. Upon comparison with the integrated mesh stiffness results derived from literature [38] taking into consideration the centre distance error, it can be seen that the variation patterns obtained in this study show a certain degree of similarity to those reported in the references. This consistency effectively validates the reliability and accuracy of the methodology proposed in this study.

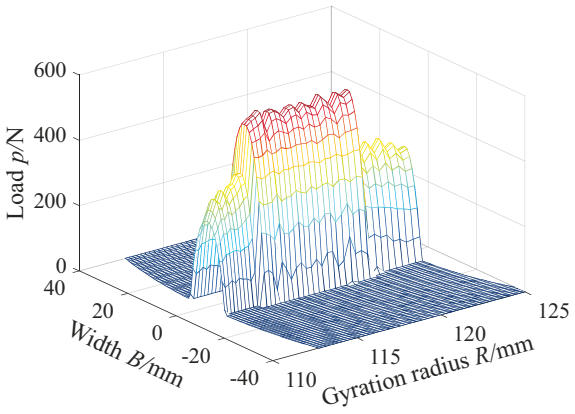

Fig. 13 Tooth surface load distribution when *De* = 3 mm

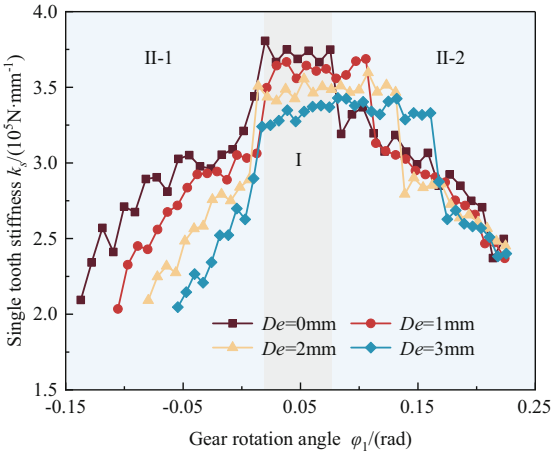

Fig. 14 Single-tooth stiffness with centre distance installation error

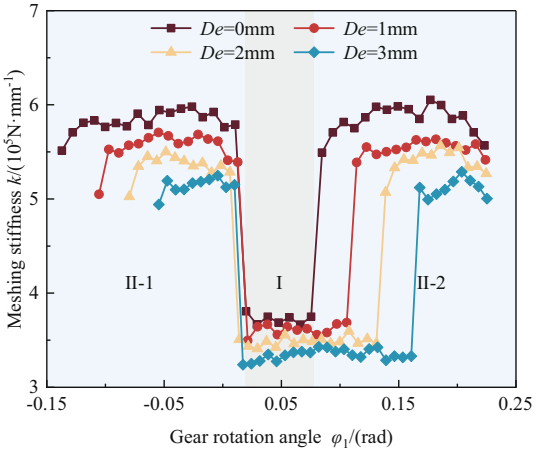

Fig. 15 Meshing stiffness with centre distance installation error

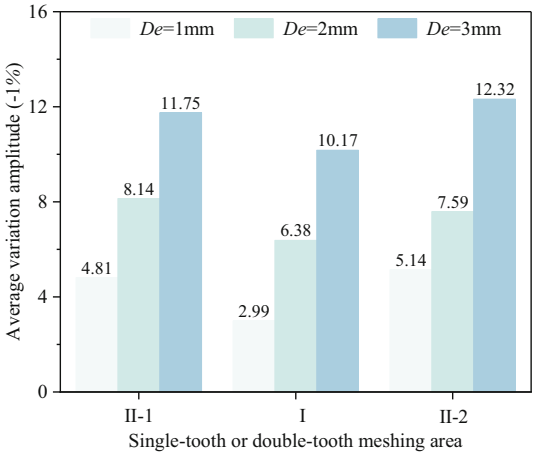

Fig. 16 Average variation amplitude of meshing stiffness

6.2 Influence of the axial installation error *Da* on meshing stiffness

Figs. 17 and 18 show the influence of *Da* on the single-tooth stiffness and meshing stiffness of the VH-CAT cylindrical gear when *Da* is 0.4 mm, 0.8 mm, and 1.2 mm, respectively. According to Figs. 17 and 18, as *Da* increases, the single-tooth stiffness and meshing stiffness of the gear decrease. Fig. 19 shows the average reduction amplitude of meshing stiffness under the influence of *Da*. The average reduction amplitude of area II-1 is 3.41%, 6.53%, and 9.94%. The average reduction amplitude of area I is 2.71%, 5.96%, and 10.65%. The average reduction amplitude of area II-2 is 2.11%, 5.11%, and 10.65%. The data show that the average reduction amplitude of the meshing stiffness increases with the axial installation error. Furthermore, the gear teeth in area II-1 are significantly impacted by axial installation errors. As the gear continues to rotate, there is a gradual decrease in the average reduction amplitude.

The main reasons are as follows: an axial installation error causes the actual meshing line of the gear to deviate from the theoretical meshing line on the middle section tooth profile, according to the structural parameters of the VH-CATT cylindrical gear, resulting in the eccentric loading and increased contact deformation of the gear pair. The increase in tooth side clearance requires greater contact deformation of the gear teeth under load to facilitate contact between the second pair of gear teeth, resulting in a greater change in contact deformation, subsequently leading to a bigger reduction in stiffness.

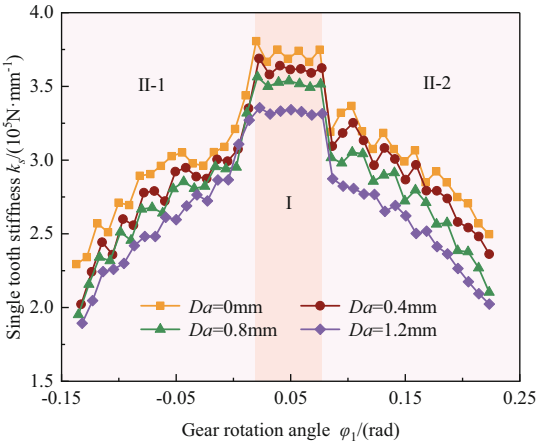

Fig. 17 Single-tooth stiffness with axial installation error

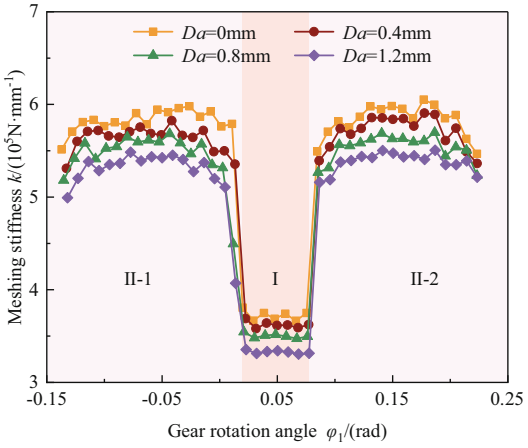

Fig. 18 Meshing stiffness with axial installation error

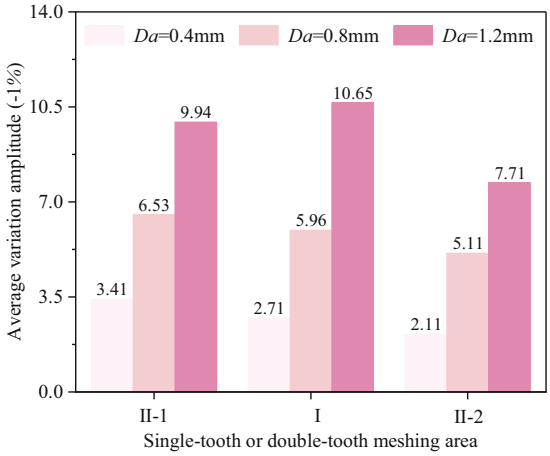

Fig. 19 Average variation amplitude of meshing stiffness

6.3 The influence of the *x*-axis rotational installation error β_x on meshing stiffness

Fig. 20 shows the influence of the *x*-axis rotational installation error β_x on the single-tooth stiffness of the VH-CATT cylindrical gear when the *x*-axis rotational installation error β_x is 0.1°, 0.2°, and 0.3°, respectively. The stiffness of a single tooth decreases with the increase of the *x*-axis rotational installation error β_x when the tooth enters the first half cycle of engagement. In the second half period of tooth engagement, the stiffness of the single tooth increases with the increase of the *x*-axis rotational installation error β_x.

Fig. 21 displays the influence of the *x*-axis rotational installation error β_x on the meshing stiffness of the VH-CATT cylindrical gear. Fig. 22 illustrates the variation amplitude of the meshing stiffness under the influence of the different *x*-axis rotational installation error β_x, which is fitted by each discrete variation amplitude point. As can be seen in Figs. 21 and 22, when the gear pair enters area II-1, area I, and area II-2, the meshing stiffness decreases first and then increases with the *x*-axis rotational installation error β_x. Fig. 23 shows the average variation amplitude of meshing stiffness under the influence of the different *x*-axis rotational installation error β_x. In area II-1, the average meshing stiffness increases, with an amplitude of 0.28%, 0.39%, and 0.62%, respectively. In area I, the average meshing stiffness is reduced, and the reduction amplitudes are 0.01%, 0.09%, and 0.16%, respectively. In area II-2, with the increase of the *x*-axis rotational installation error β_x, the average meshing stiffness first increases

and then decreases. The change amplitudes corresponding to β_x of 0.1°, 0.2°, and 0.3° are 0.18%, 0.07%, and-0.18%, respectively. However, in general, the rotational installation error around the x-axis has little effect on the meshing stiffness of the VH-CATT cylindrical gear system.

The aforementioned occurrence is caused by the fact that the gear's initial meshing point is far from the middle section when the x-axis rotational installation error β_x occurs, and the degree of deviation declines as the pinion's rotational angle increases. The closer the actual meshing line is to the middle section of the gear tooth, the smaller the contact deformation. Moreover, with the increase of the x-axis rotational installation error β_x, the load increases toward the top of the tooth and declines near the base.

Simultaneously, it can be observed in Fig. 24 that as the gear tooth is on the verge of exiting the double-tooth meshing area II-1 and of entering the single-tooth meshing area I, a larger x-axis rotational installation error β_x leads to greater mutation in meshing stiffness. This phenomenon arises due to the significant alternation in the contact load between the front and rear teeth of single and double teeth.

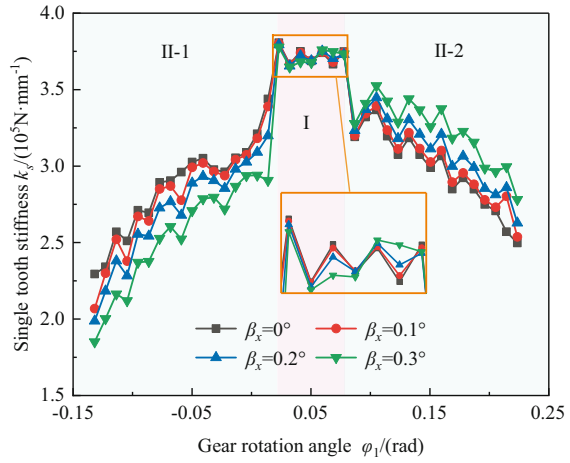

Fig. 20 Single-tooth stiffness with x-axis rotational installation error

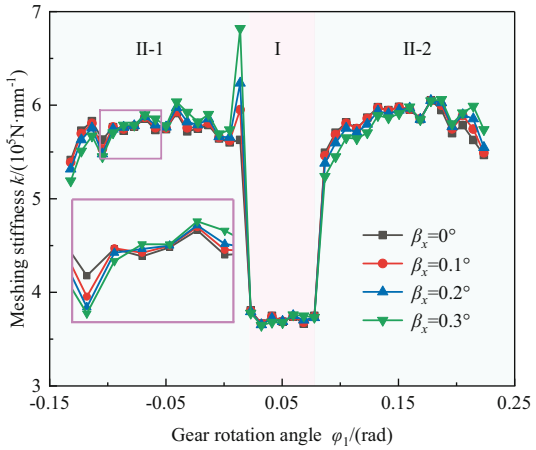

Fig. 21 Meshing stiffness with x-axis rotational installation error

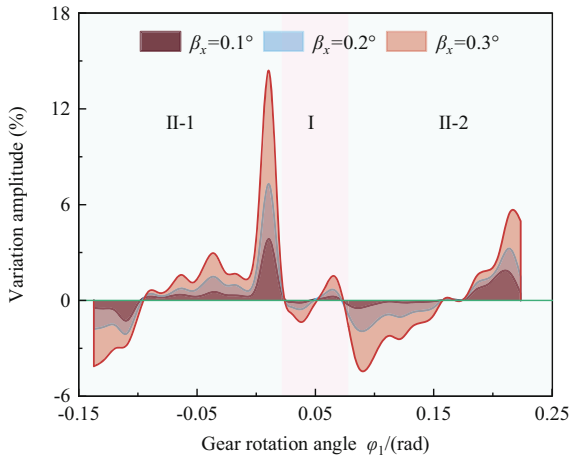

Fig. 22 Meshing stiffness variation amplitude

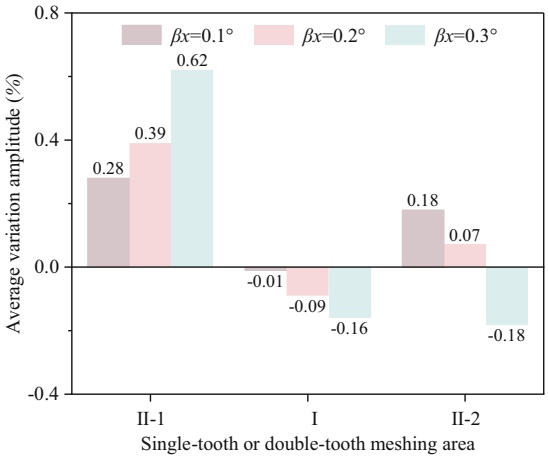

Fig. 23 Average variation amplitude of meshing stiffness

6.4 The influence of the *y*-axis rotational installation error on meshing stiffness

Fig. 24 shows the influence of the *y*-axis rotational installation error β_y on the single-tooth stiffness of the VH-CATT cylindrical gear when the *y*-axis rotational installation error β_y is 0.1°, 0.2°, and 0.3°, respectively. As depicted in the figure, during the initial phase of the tooth engagement cycle, the single-tooth stiffness exhibits a notable increase in response to a rise in the installation error β_y. In the second half period of tooth engagement, the stiffness of the single tooth decreases with the increase of the rotational installation error β_y around the *y*-axis.

Fig. 25 shows the influence of the *y*-axis rotational installation error β_y on the meshing stiffness of the VH-CATT cylindrical gear. The variation amplitude of the meshing stiffness under the influence of the different *y*-axis rotational installation error β_y is shown in Fig. 26. From Figs. 25 and 26, it is evident that as the gear pair enters area II-1, area I, and area II-2, the meshing stiffness initially increases and then decreases with an increase in the *y*-axis rotational installation error β_y. Fig. 27 displays the average change amplitude of the meshing stiffness under the influence of the different *y*-axis rotational installation error β_y. From the figure, it can be seen that the average meshing stiffness is reduced. In area II-1, the reduction amplitudes are 0.37%, 0.81%, and 1.46%, respectively. In area I, the reduction amplitudes are 0.04%, 0.18%, and 1.13%, respectively. In area II-2, the reduction amplitudes are 0.35%, 1.71%, and 2.96%, respectively. However, it can be seen from Figs. 24 and 25 that the fluctuation range of single-tooth stiffness and meshing stiffness is relatively large.

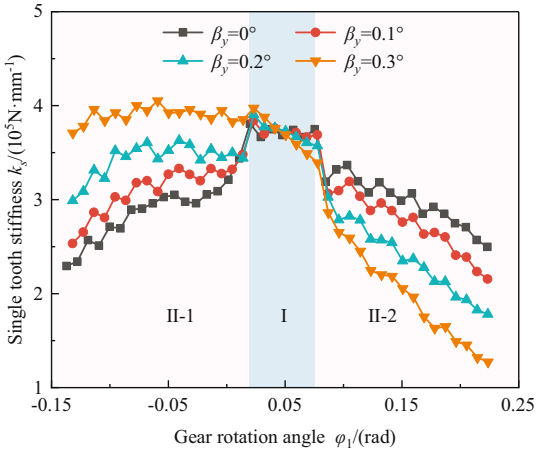

Fig. 24 Single-tooth stiffness with *y*-axis rotational installation error

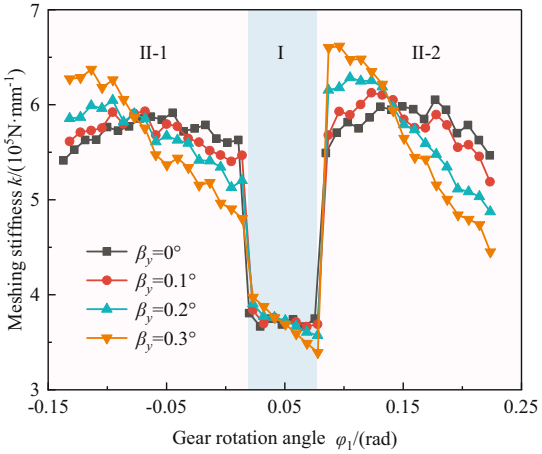

Fig. 25 Meshing stiffness with *y*-axis rotational installation error

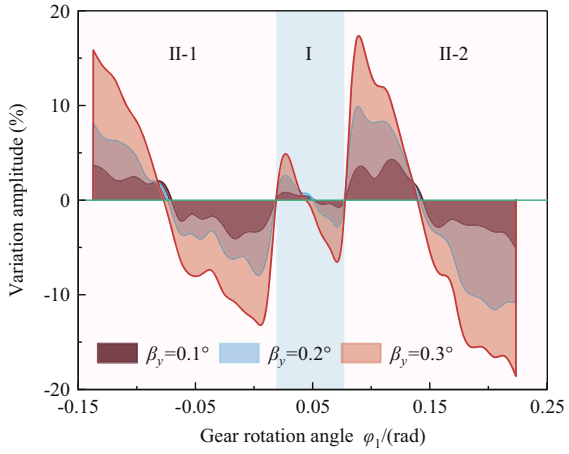

Fig. 26 Meshing stiffness variation amplitude

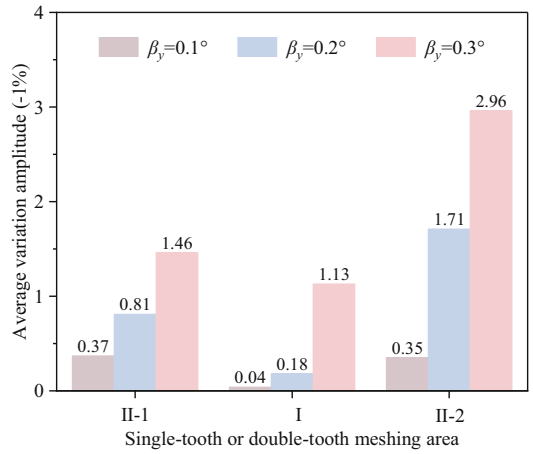

Fig. 27 Average variation amplitude of meshing stiffness

The aforementioned phenomenon stems from the fact that in the presence of a *y*-axis rotational installation error, the actual meshing line of the gear diverges from the theoretical meshing line at the midpoint. As the pinion's rotational angle escalates, the degree of deviation intensifies, causing the gear meshing point to extend towards the end face of the tooth, ultimately leading to a reduction in the amount of contact deformation. Moreover, with the increase of the rotational installation error around the *y*-axis, the load near the root of the tooth increases, the load near the top of the tooth decreases, and the load difference between the teeth is large.

Fig. 25 reveals that as the gear tooth approaches the transition from area I to area II-2, a larger *y*-axis rotational installation error β_y correlates with more pronounced mutation. This is attributed to the fact that in area II-2 of the gear system, the first pair of meshing teeth carries a relatively minor load, whereas the second pair assumes most of the load. Consequently, this transition from single- to double-tooth engagement elicits an amplification in the difference of contact deformation within the gear system.

7. Conclusion

This paper, leveraging a combined model integrating tooth contact analysis (TCA) with misalignment errors and loaded tooth contact analysis (LTCA), computes the tooth surface load distribution under loading conditions for VH-CATT cylindrical gears. Furthermore, it calculates the single-tooth stiffness and mesh stiffness of VH-CATT cylindrical gears. Finally, the study examines the influence of various misalignment errors on the single-tooth stiffness and mesh stiffness of VH-CATT cylindrical gears. The key findings are summarised as follows:

1. In order to calculate the load distribution and meshing stiffness of VH-CATT cylindrical gears under installation errors, a calculation method combining the TCA model and LTCA model with installation errors is proposed. The theoretical analysis is in excellent agreement with the computational results, thereby validating the accuracy and reliability of the proposed method.
2. When installation errors arise, the meshing stiffness of VH-CATT cylindrical gears undergoes notable alterations. For instance, a centre distance installation error results in a decrease in both single-tooth stiffness and meshing stiffness, accompanied by an expansion of the single-tooth meshing area within the gear system and the emergence of a hysteresis phenomenon during meshing. Additionally, axial installation errors lead to a reduction in both these stiffness parameters, with the decremental amplitude becoming more pronounced as the error magnifies. The rotational installation error around the normal direction of the gear centre line (for the x-axis) significantly affects the distribution of single-tooth stiffness, specifically causing a decrease in stiffness at the tooth root and an increase at the tooth tip, albeit with minimal consequences for the overall meshing stiffness. However, rotational installation errors around the gear centre line direction (for the y-axis) exert substantial influence on both single-tooth stiffness and meshing stiffness, resulting in an increase in stiffness near the tooth root, a decrease near the tooth tip, and substantial fluctuations in meshing stiffness.
3. This paper offers a thorough examination of the meshing stiffness characteristics in the context of installation errors. The study conclusively demonstrates that the meshing stiffness of the gear system is profoundly influenced by installation errors. To enhance the transmission performance of the gear system, it is crucial to meticulously avoid any installation errors during the installation of the gear pair.

Acknowledgements

This work was supported by the National Natural Science Foundation of China (Grant No. 52105058), the Innovation Project of Lanzhou Youth Science and Technology Talent (No. 2023-QN-43), the Guizhou Provincial Science and Technology Projects (No. Qiankehejichu - ZK [2021] yiban 273), the Zunyi Normal University Doctor Fund (Zunshi BS [2024] 03Hao), and the Zunyi Science and Technology Plan Project (Zunshikehe HZ Zi [2024] 139Hao).

REFERENCES

[1] Ma Dengqiu, Ye Zhenhuan, Yang Hang. Tooth surface reconstruction and tooth profile geometric analysis of circular arc tooth trace cylindrical gears. Transactions of FAMENA 2019, 43(1), 29-44. https://doi.org/10.21278/TOF.43103

[2] Zhao Fei, Hou Li, Chen Y, Luo Lan. Mathematical model and generating condition analysis of cylindrical gear with circular-arc-tooth-trace. Journal of Jilin University (Engineering and Technology Edition) 2020, 50(03), 875-885. https://doi.org/10.13229/j.cnki.jdxbgxb20190058

[3] Zhang Haiyan, Hou Li, Luo Lan, Liang Shuang, Len Song. Modular Design for Machine Tools of Variable Hyperbolic Circular-arc-tooth-trace Cylindrical Gear. Journal of Mechanical Engineering 2021, 57(3), 77-86. https://doi.org/10.3901/JME.2021.03.077

[4] Zhang Haiyan, Hou Li, Liang Shuang, Wu Yang, Chen Zhongmin. Modular configuration design of a special machine tool for variable hyperbolic circular-arc-tooth-trace cylindrical gears. Mechanical Sciences 2020, 13(1), 55-65. https://doi.org/10.5194/ms-13-55-2022

[5] Wu Yang, Hou Li, Luo Lan, Ma Dengqiu, Wei Yongqiao, Yi Zongli. Research on the Effect Law of Machine Tool Errors on Tooth Surface Errors of Curvilinear Gear. Journal of Mechanical Engineering 2020, 56(21), 100-109. https://doi.org/10.3901/JME.2020.21.100

[6] Wu Yang, Hou Li, Ma Dengqiu, Wei Yongqiao, Luo Lan. Milling Machine Error Modelling and Analysis in the Machining of Circular-Arc-Tooth-Trace Cylindrical Gears. Transactions of FAMENA 2020, 44(4), 13-29. https://doi.org/10.21278/TOF.444009419

[7] Wu Yang, Luo Pei, Bai Qingsong, Liang Shuang, Fan Qingwen, Hou Li. Modelling and analyzing of loaded meshing characteristics of cylindrical gear transmission with curvilinear-shaped teeth. Meccanica 2023, 58(8), 1555-1580. https://doi.org/10.1007/s11012-023-01690-1

[8] Guo Rui, Wei Yongqiao, Liu Yongping, Li Dawei, Yang Dong, Zhao Gang. Analytical solution to contact characteristics for a variable hyperbolic circular-arc-tooth-trace cylindrical gear. Mechanical Sciences 2021, 12(2), 923-932. https://doi.org/10.5194/MS-12-923-2021

[9] Liu Yongping, Ma Dengqiu. Surface modification and tooth contact analysis of variable hyperbolic circular-arc-tooth-trace cylindrical gears. Mechanical Sciences 2022, 13(2), 909-920. https://doi.org/10.5194/MS-13-909-2022

[10] Liang Shuang, Hou Li, Zhang Haiyan, Luo Lan, Wu Yang, Luo Pei. Bifurcation and chaos analysis of cutter head-spindle system of VH-CATT gear machine tool considering time-varying stiffness. The International Journal of Advanced Manufacturing Technology 2022, 124(11-12), 1-14. https://doi.org/10.1007/s00170-021-08360-0

[11] Liang Shuang, Wu Yang, Hou Li, Dong Lei, Fan Qingwen, Zhang Haiyan. Research on influence mechanism of geometric error sources on tooth surface error of VH-CATT gear special machine tool. The International Journal of Advanced Manufacturing Technology 2023, 128(11-12), 5529-5546. https://doi.org/10.1007/s00170-023-12001-z

[12] Wei Yongqiao, Yang Dong, Guo Rui, Ren Zhongtao, Li Zeyu, Luo Lan. Integrated wear prediction model for cylindrical gear with variable hyperbolic circular arc tooth trace under mixed elastohydrodynamic lubrication. Journal of Mechanical Science and Technology 2022, 36(8), 4053-4065. https://doi.org/10.1007/S12206-022-0726-1

[13] Wei Yongqiao, Yang Dong, Guo Rui, Liu Yongping, Luo Lan, Li Zeyu. Wear characteristics analysis of variable hyperbolic circular-arc-tooth-trace cylindrical gear transmission considering assembly error theory. Proceedings of the Institution of Mechanical Engineers, Part J: Journal of Engineering Tribology 2024, 238(4), 399-413. https://doi.org/10.1177/13506501231218493

[14] Ma Dengqiu, Liu Yongping, Ye Zhenhuan, Wei Yongqiao, Liu Jing. Analysis of the Tooth Surface Contact Area of a Circular-Arc-Tooth-Trace Cylindrical Gear under Load. Transactions of FAMENA 2021, 45(1), 79-94. https://doi.org/10.21278/TOF.451018220

[15] Ma Dengqiu, Liu Yongping, Ye Zhenhuan, Wei Yongqiao, Li Dawei, Zhang Xu. Meshing Contact Impact Properties of Circular Arc Tooth Trace Cylindrical Gear Based on Rotating Knife Dish Milling Process. Mathematical Problems in Engineering 2021,8819818. https://doi.org/10.1155/2021/8819818

[16] Ma Dengqiu, Liu Yongping, Ye Zhenhuan, Li Dawei, Wu Yang. Influence of Cutter Errors on Forming Accurate Variable Hyperbolic Circular Arc Tooth Trace Cylindrical Gears. Transactions of FAMENA 2023, 47(4), 13-31. https://doi.org/10.21278/TOF.474044222

[17] Ma Dengqiu, Liu Yongping, Ye Zhenhuan, Li Dawei, Wei Yongqiao. Modification design and load tooth contact analysis of a cylindrical gear with variable hyperbolic circular arc tooth trace. Journal of Vibration and Shock 2023, 42 (14), 170-179. https://doi.org/10.13465/j.cnki.jvs.2023.14.020

[18] Luo Yang, Baddour Natalie, Liang Ming. Effects of gear center distance variation on time varying mesh stiffness of a spur gear pair. Engineering Failure Analysis 2017, 75, 37-53. https://doi.org/10.1016/j.engfailanal.2017.01.015

[19] Shehata Ahmed, Adnan Md Asif, Mohammed Omar D. Modeling the effect of misalignment and tooth microgeometry on helical gear pair in mesh. Engineering Failure Analysis 2019, 106, 104190-104190. https://doi.org/10.1016/j.engfailanal.2019.104190

[20] Kumar Paras, Hirani Harish, Agrawal Kumar Atul. Effect of gear misalignment on contact area: Theoretical and experimental studies. Measurement 2019, 132, 359-368. https://doi.org/10.1016j.measurement.2018.09.070

[21] Kumar Paras, Hirani Harish. Misalignment effect on gearbox failure: An experimental study. Measurement 2021, 169, 108492. https://doi.org/10.1016/j.measurement.2020.108492

[22] Lü Hongzhan, Wang Yuda, Wang Junzheng. Loaded Tooth Contact Analysis of Spur Gears with Longitudinal Modification Considering Assembly Errors. Journal of Mechanical Engineering 2022, 58(21), 126-133. https://doi.org/10.3901/JME.2022.21.126

[23] Song Chaosheng, Xia Maohao, Liu Siyuan, Liang Chengcheng. Influences of machine-tool setting errors on mesh behavior for small-module spiral bevel gear. Journal of Mechanical Science and Technology 2022, 36(9), 4523-4533. https://doi.org/10.1007/S12206-022-0816-0

[24] Zhao Zhifang, Yang Yang, Ma Hui, Wang Haixu, Tian Hongxu, Han Chenyi. Meshing characteristics of spur gear pairs with tooth modification under different assembly errors and sensitivity analysis for impact factors. Journal of Mechanical Science and Technology 2022, 37(1), 149-162. https://doi.org/10.1007/S12206-022-1215-2

[25] Li Haonan, Chen Siyu, Tang Jinyuan, Sun Zhou, Hu Youwang. Nonlinear dynamic modeling and analysis of spur gear based on gear compatibility conditions. Mechanism and Machine Theory 2022, 171, 104767. https://doi.org/10.1016/j.mechmachtheory.2022.104767

[26] Sun Zhou, Chen Siyu, Hu Zehua, Tao Xuan. Improved mesh stiffness calculation model of comprehensive modification gears considering actual manufacturing. Mechanism and Machine Theory 2022, 167, 104470. https://doi.org/10.1016/j.mechmachtheory.2021.104470

[27] Kong Xiannian, Hu Zehua, Tang Jinyuan, Chen Siyu, Wang Zhiwei. Effects of gear flexibility on the dynamic characteristics of spur and helical gear system. Mechanical Systems and Signal Processing 2023, 184, 109691. https://doi.org/10.1016/j.ymssp.2022.109691

[28] Marafona João D.M., Marques Pedro M.T., Portron Stéphane, Martins Ramiro C., Seabra Jorge H.O. Gear mesh stiffness and dynamics: Influence of tooth pair structural stiffness asymmetry. Mechanism and Machine Theory 2023, 190, 105447. https://doi.org/10.1016/J.mechmachtheory.2023.105447

[29] Pedrero José I., Pleguezuelos Miguel, Sánchez Miryam B. Analytical model for meshing stiffness, load sharing, and transmission error for helical gears with profile modification. Mechanism and Machine Theory 2023, 185, 105340. https://doi.org/10.1016/j.mechmachtheory.2023.105340

[30] Jianmin Wen, Haoyu Yao, Qian Yan, Bindi You. Research on Time-Varying Meshing Stiffness of Marine Beveloid Gear System. Mathematics 2023, 11(23), 4774. https://doi.org/10.3390/math11234774

[31] Zou Desheng, Wang Liming, Ye Hui, Yu Wennian, Pan Wenchao, Shao Yimin, Chris Mechefske. Spur gear time-varying mesh stiffness considering meshing phase difference caused by angle misalignment error. Meccanica 2024, 59(3), 475-490. https://doi.org/10.1007/s11012-024-01762-w

[32] Liu Ziqian, Jiang Yanjun, Luo Ruitian, Wu Yangda, Huang Jiaopeng, Feng Nan, Li Kui. Improved analytical model for calculating mesh stiffness and transmission error of helical gears considering root curve: Theoretical analysis and experiments. Advances in Mechanical Engineering 2024, 16(2), 1-22. https://doi.org/10.1177/16878132241228196

[33] Cai Zhijie, Zheng Xiqing, Lan Huiqing, Wang Liuna, Yang Siwei, Sheng Rui. Time-Varying Meshing Stiffness and Dynamic Parameter Model of Spiral Bevel Gears with Different Surface Roughness. Applied Sciences 2024, 14(4), 1533. https://doi.org/10.3390/app14041533

[34] Li Zhanwei, Zhang Juntao, Song Hansheng, Zhu Rupeng, Ma Hui. Time-varying mesh stiffness calculation of spiral bevel gear with spalling defect. Mechanism and Machine Theory 2024, 193, 105571. https://doi.org/10.1016/j.mechmachtheory.2023.105571

[35] Li Haonan, Tang Jinyuan, Chen Siyu, Ding Han, Sun Zhou, Rong Kaibin. Analytical calculation of mesh stiffness for spiral bevel gears with an improved global tooth deformation model. Mechanism and Machine Theory 2024, 191, 105492. https://doi.org/10.1016/j.mechmachtheory.2023.105492

[36] Sánchez Miryam B., Pleguezuelos Miguel, Pedrero José I. Influence of profile modification on the transmission error of spur gears under surface wear. Mechanism and Machine Theory 2024, 191, 105473. https://doi.org/10.1016/j.mechmachtheory.2023.105473

[37] Ma Dengqiu, Jiang Bing, Bao Lingli, Ye Zhenhuan, Liu Yongping. Study on the contact performance of the variable hyperbolic circular arc tooth trace cylindrical gear with installation errors. Mechanical Sciences 2024, 15(1), 353-366. https://doi.org/10.5194/ms-15-353-2024

Submitted: 31.7.2024

Accepted: 24.9.2025

Bing Jiang
Yongqiao Wei*
School of Mechanical and Electrical Engineering, Lanzhou University of Technology, Lanzhou, 730050, China

Shaojiang Wang
Sinomach Heavy Equipment Group Co., Ltd, Deyang 618099, China

Jianquan Zhang
The Second Research Institute of Civil Aviation Administration of China, Chengdu, China

Dengqiu Ma
School of Engineering and Technology, Zunyi Normal College, Zunyi, 563006, China

Lan Luo
School of Mechanical and Electrical Engineering, Lanzhou University of Technology, Lanzhou, 730050, China

Jianbing Long
Guizhou Qun Jian Precision Machine Co., Ltd, Zunyi, 563003, China

*Corresponding author:
scuwyq@163.com